Contents

List of Figures

List of Tables

1 Overview of the Experiment

In this experiment the we investigate the γ spectrum of the decay chain of the thorium isotope ^{228}Th and verify the occurrence of electron-positron pair annihilation by examining the angular correlation of temporally coinciding photons of energy 0.511MeV. To calibrate the Energy measurement, the Isotopes ^{22}Na, ^{152}Eu and ^{60}Co are used, whose spectra are given in [1].

2 Theoretical Introduction

The information in this chapter is taken from [2] if not specified otherwise.

2.1 Radioactive Decay

2.1.1 α Decay

An α particle can be emitted by an ${}^{A}_{Z}\mathrm{X}$ according to the following reaction:

$$ {}^{A}_{Z}\mathrm{X} \longrightarrow {}^{A-4}_{Z-2}\mathrm{Y} + \alpha \tag{1} $$

The α particle is a ${}^{4}_{2}$He nucleus which has a charge of $+2e$. The α particle is bound to the original nucleus by a Coulomb barrier which, according to classical electromagnetism theory, it does not have sufficient energy to surmount. The decay can be explained by quantum tunneling, where the wave function of the α particle penetrates the barrier with an exponentially decreasing amplitude which leads to a non-zero transmission probability.

2.1.2 β Decay

β decay can be observed in three different phenomena:

β^- decay: In the β^- decay, a neutron in the nucleus transforms into a proton under emission of an electron and an anti-electron-neutrino according to the following reaction:

$$ n \longrightarrow p + e^- + \overline{\nu}_e \tag{2} $$

This means that the original nucleus ${}^{A}_{Z}\mathrm{X}$ becomes ${}^{A}_{Z+1}\mathrm{Y}$.

β^+ decay: In the β^+ decay, a neutron in the nucleus transforms into a proton under emission of a positron and an electron-neutrino according to the following reaction:

$$ p \longrightarrow n + e^+ + \nu_e \tag{3} $$

This means that the original nucleus ${}^{A}_{Z}\mathrm{X}$ becomes ${}^{A}_{Z-1}\mathrm{Y}$.

Electron Capture: The nucleus captures an electron from its closest shell which transforms a proton on the nucleus into a neutron under emission of an electron-neutrino:

$$ p + e^- \longrightarrow n + \nu_e \tag{4} $$

2.1.3 γ Decay

In the aforementioned α and β decays, the resulting nucleus is usually left in an excited state which then relaxes into the ground state. If the excitation energy is not large enough to emit a particle, it is emitted by a quantum of electromagnetic γ radiation which is a photon of typical energies of keV to MeV.

Internal Conversion: Another phenomenon that can occur during the relaxation of an excited nucleus is the so-called internal conversion, where the excess energy is not emitted as a Photon but absorbed by an Electron in the atomic shell which then has enough energy to surmount its binding energy and is emitted from the atom. The hole which is left by the emitted electron is filled by an electron from an energetically higher shell. The energy difference between the shells for its part can be emitted as X-radiation or by emission of another electron which is then called Auger electron.

Pair annihilation: The Positron which is emitted in β^+ decay is decelerated by matter and then forms a bound state with an electron which is called positronium. The positronium is unstable and decays under emission of two or three photons:

$$e^+ + e^- \longrightarrow 2\gamma \tag{5}$$

$$\text{or} \quad e^+ + e^- \longrightarrow 3\gamma \quad , \tag{6}$$

where the decay into two photons is much more probable than the decay into three photons. Conservation of momentum implies that the angle between the two photons must be 180° and from the energy-momentum-relation,

$$E^2 = p^2c^2 + m^2c^4 \quad , \tag{7}$$

it is known that both photons have an energy of

$$E_\gamma = 0.511\text{MeV} \tag{8}$$

2.2 Interaction of Electromagnetic Radiation With Matter

The interaction of electromagnetic radiation with matter, which is responsible for the attenuation of gamma rays by matter, mainly consists of three phenomena that are explained in this section.

2.2.1 Photoelectric Effect

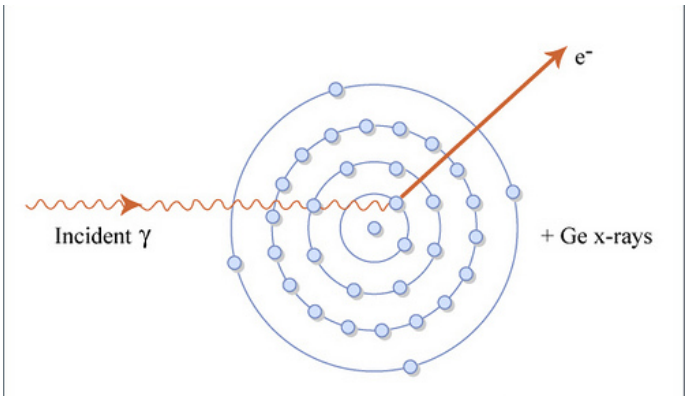

Figure 1: Schematic depiction of the photoelectric effect [4]

The energy of a photon is absorbed by a bound electron in the atomic shell. If the photon's energy $E_\gamma = h\nu$ is greater than the work function W, that is, the minimal energy required to remove an electron from its binding to the atom, the electron is emitted with the kinetic energy $E_e = E_\gamma - W$. Analogously to the internal conversion described in section 2.1.2, the atom emits X-radiation or an Auger electron. The photoelectric effect is depicted schematically in figure 1.

2.2.2 Compton Scattering

The inelastic scattering of a photon and a charged particle (in this case an electron in the atomic shell) is called Compton scattering. The Photon transfers a part of its energy to the electron and thereby experiences a red-shift. A typical γ spectrum involving Compton scattering is shown in fig. 2.

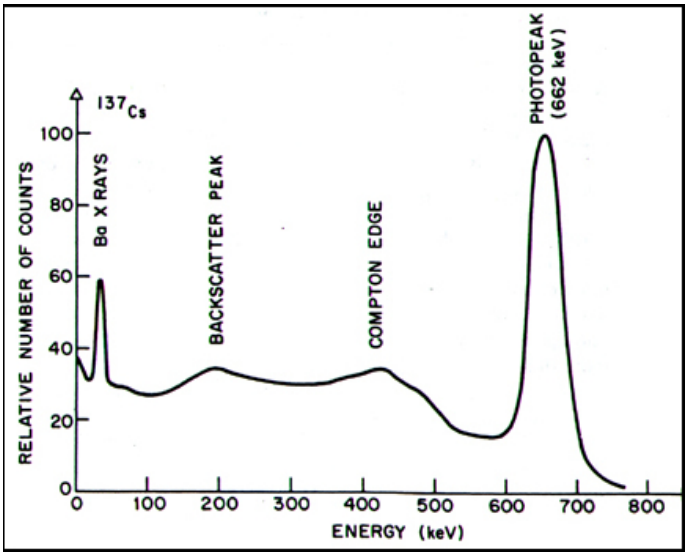

Figure 2: Gamma spectrum of the ^{137}Cs isotope [5]

The energy of the scattered photon depends on the scattering angle, which means that the Compton spectrum has two sharp edges: The backscatter edge, where a maximum amount of energy is transferred from the incoming photon to the electron, and the Compton edge, where the transferred energy is minimal. Fig. 2 also shows the ^{137}Cs photopeak which comes from a complete absorption of the photon energy by the scintillation crystal (cf. sec. 2.3).

2.2.3 Pair Creation

If a photon has got at least twice the rest energy $E = m_e c^2 = 0.511\text{MeV}$ [2] of an electron, it can produce an electron-positron pair. The energy-momentum-relation (eq. 7) implies that pair creation can only take place nearby a nucleus. The positron produced in pair production is then annihilated as described in section 2.1.2.

2.3 Scintillator

A scintillator is a material which is used to detect photons exploiting its luminescence property. The basic principle of a scintillator is that it changes into an excited electronic state by absorption of a photon and emits another photon while relaxing

back into the ground state, which can then be detected. In this experiment, two types of scintillators are used:

Inorganic Scintillator: An inorganic scintillator has a lattice structure. An absorbed photon causes a collective lattice excitation of the crystal. By solving the stationary Schrödinger equation for a periodic potential, one can show that the atoms in a crystalline material have got collective energy bands (cf. fig. 3).

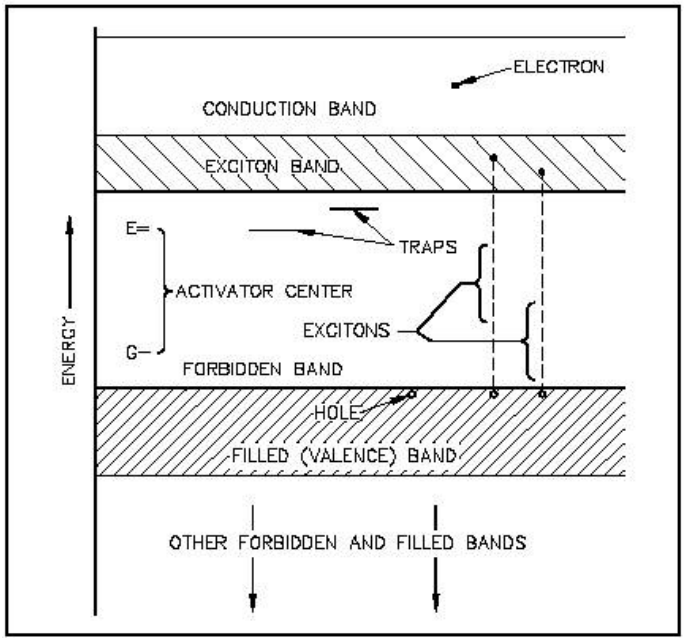

Figure 3: Band structure of a doped scintillation crystal [6]

An electron in the valence band can be excited into the conduction band where it moves freely and the crystal becomes a conductor. In the valence band there remains a hole which also moves freely through the crystal. An electron that is excited by a photon but does not absorb enough energy to reach the conduction band, is still loosely bound to the hole. This electron-hole-pair is called an exciton and can also move freely inside the crystal. When the electrons relax into the valence band, another photon is emitted. To be able to detect this photon, it has to be made sure that it is not re-absorbed by the crystal. This is achieved by doping the crystal with activator atoms. This so called activator impurity locally deforms the conduction band and creates new energy levels. The electrons, holes and excitons move through the crystal until they reach such an impurity, where they recombine emitting a photon which hasn't got enough energy to excite a valence electron into the conduction band. Therefore these activator photons can pass through the crystal and be detected.

Organic Scintillator: In an organic scintillator, the activator substance is dissolved in the carrier substance (in this case plastic). The solvent is excited by an incoming photon. The excitation energy is passed onto the activator which re-emits another photon which, analogously to the inorganic case, has got the appropriate energy to pass through the material and be detected afterwards.

Compared to an organic scintillator, the inorganic one has got a better energy resolution due to a more efficient transformation of the excitation energy into luminescence light. On the other hand, the organic scintillator has got a better time resolution since the excitation and relaxation of atoms and molecules takes place at a time scale of nanoseconds, while the lattice excitations of an inorganic scintillator take place with a time constant of up to 100μs.

2.4 Isotopes Used in the Experiment

2.4.1 ^{22}Na

$^{22}_{11}$Na decays via β^- decay into the excited state 2^+ of $^{22}_{10}$Ne with a probability of nearly 100% and a half life of 2.6088years, Where the β^+ decay

$$^{22}_{11}\mathrm{Na} \longrightarrow {}^{22}_{10}\mathrm{Ne} + \nu_e \tag{9}$$

takes place with a probability of 89.9 % and the electron capture

$$^{22}_{11}\mathrm{Na} + e^- \longrightarrow {}^{22}_{10}\mathrm{Ne} + \nu_e \tag{10}$$

takes place with a probability of 10.1 %. The decay scheme of $^{22}_{11}$Na is shown in fig. 4.

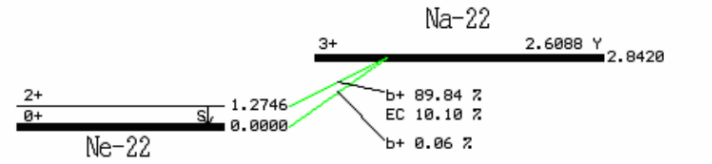

Figure 4: Decay scheme of ^{22}Na [2]

2.4.2 ^{152}Eu

$^{152}_{63}$Eu decays via β decay with a half life of 12 years. All three types of β decay occur:

$$^{152}_{63}\mathrm{Eu} \longrightarrow {}^{152}_{64}\mathrm{Gd} + e^- + \overline{\nu}_e \qquad (\beta^-) \tag{11}$$

$$^{152}_{63}\mathrm{Eu} \longrightarrow {}^{152}_{62}\mathrm{Sm} + e^+ + \nu_e \qquad (\beta^+) \tag{12}$$

$$^{152}_{63}\mathrm{Eu} + e^- \longrightarrow {}^{152}_{62}\mathrm{Sm} + \nu_e \qquad (\mathrm{EC}) \tag{13}$$

Figure 5 shows a simplified version of the $^{152}_{63}$Eu isotope which only contains the two most intense γ transitions.

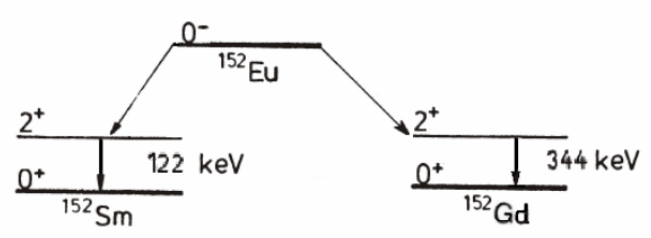

Figure 5: Simplified decay scheme of ^{152}Eu [2]

2.4.3 ^{60}Co

$^{60}_{27}$Co decays via β^- decay with a half life of 5.2714years and a probability of nearly 100% into the excited state 4^+ of $^{60}_{28}$Ni:

$$^{60}_{27}\mathrm{Co} \longrightarrow {}^{60}_{28}\mathrm{Ni} + e^- + \overline{\nu}_e \tag{14}$$

Figure 6 shows the decay scheme of $^{60}_{27}$Co.

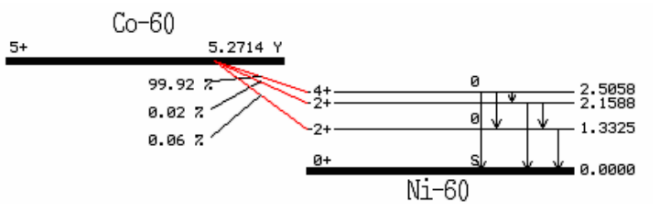

Figure 6: Decay scheme of ^{60}Co[2]

2.4.4 ^{228}Th

In the decay chain of ^{228}Th (cf. fig. 7), α, β and γ decays occur.

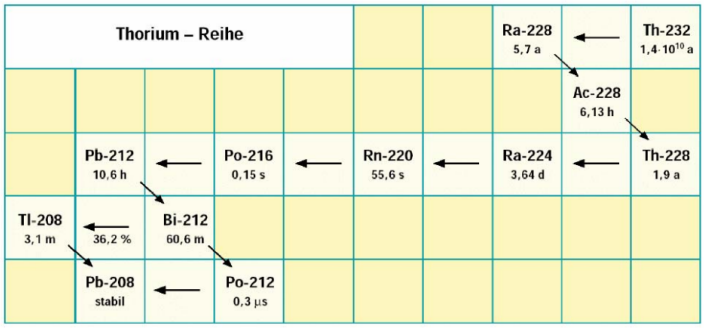

Figure 7: Decay Chain of ^{232}Th (includes the decay chain of ^{228}Th) [2]

A selection of γ-peaks of the ^{228}Th decay chain which are relevant for this experiment is shown in appendix 6.1.

2.5 Electronic Devices [3]

2.5.1 Photomultiplier

Via the photoelectric effect, electrons are emitted from the photocathode when they absorb a photon of sufficient energy. Various dynodes and acceleration voltages cause the production of many more electrons which reach the anode and can then be detected as a pulse of electric current. The number of electrons that reach the anode depends on the material of the dynodes and the acceleration voltage. The photomultiplier is schematically displayed in fig. 8 .

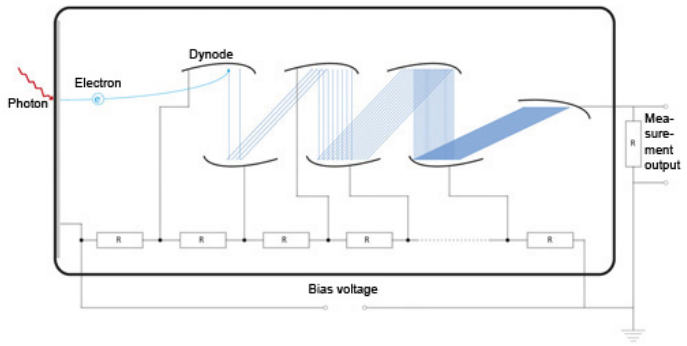

Figure 8: Schematic setup of a photomultiplier [7]

2.5.2 Pre-Amplifier

The pre-amplifier integrates the electric current from the photomultiplier to obtain a voltage signal whose amplitude is proportional to the number of electrons which reach the anode of the photomultiplier. The output signal has a short increase and a decrease which is by a factor of around 100 times slower.

2.5.3 Main Amplifier

The amplification level can be controled by the *gain* controller (and the *coarse gain* for adjustment on a higher scale). The *Shaping Time* controller determines the shape of the output signal. Within the adjusted shaping time interval, the maximum amplitude is determined. The shaping time should be elected to be long enough to reach the maximum amplitude but short enough to reduce the dead time resulting from the delay of the output signal by the shaping time. There are two modes of the output signal: The unipolar output, which delivers a gaussian-shaped signal and the bipolar output, which delivers a dispersion curve.

2.5.4 Multi Channel Analyzer

The multi channel analyzer measures the height of an incoming pulse by comparing it with a sawtooth voltage signal. The pulses are then distributed into an adjustable number of channels, sorting them by their height. In the experiment, after an energy calibration, the channels can be assigned with a corresponding energy each.

2.5.5 Timing Single Channel Analyzer

The single channel analyzer only detects incoming signals with a certain amplitude window. The amplitude window can be adjusted with a *lower level* and a *upper level* controller. In the experiment, the amplitude window is adjusted for the equipment to only detect photons within a certain energy frame. The output of the SCA is a logical rectangular signal. The input and output signal and the influence of the amplitude window is visualized in fig. 9.

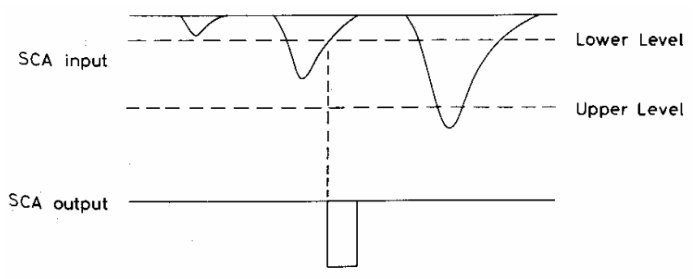

Figure 9: Input and output signal of the single channel analyser [3]

The output signal can be delayed relatively to the input signal using the *delay* controller.

2.5.6 Coincidence Unit

The coincidence unit checks if two incoming signals have got a temporal overlap. In this case it delivers a logical signal to the output. This is visualized in fig. 10.

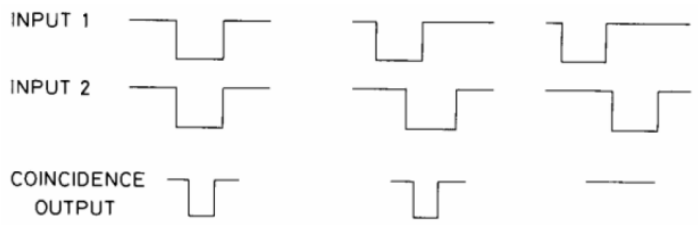

Figure 10: Different possibilities of the input and output signal of the coincidence unit [3]

3 Experimental Setup and Excecution

3.1 Energy Spectra

A block diagram representing the electronic circuit for the measurement of energy spectra is shown in fig. 11.

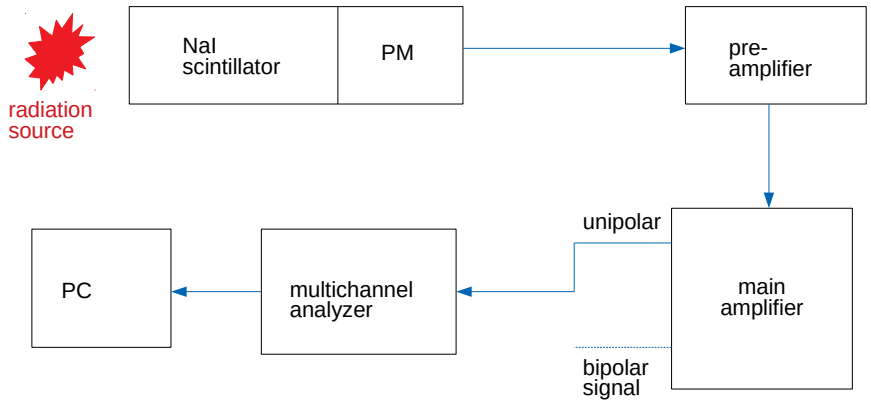

Figure 11: Block diagram representing the electronic circuit for the measurement of energy spectra

In this part of the experiment an inorganic NaI scintillator is directly attached to a photomultiplier (PM). A pre-amplifier is built into the PM. The signal from the unipolar output of the main amplifier is goes to the multi channel analyzer which then transmits it to a computer (PC). The PC has a measurement software installed with which measurements can be performed and the number of channels of the multi channel analyzer can be adjusted. The software displays the currently measured spectrum in real time.

The number of channels in the multi channel analyzer is set to 4089. The parameters at the main amplifier are set as follows:

course gain:	50
gain:	6.99 ± 0.05
shaping time:	3 μs

The parameters and the number of channels were adjusted so the Thorium peak at around 2.6 MeV was well visible on the computer screen.

The γ spectra of ^{22}Na, ^{60}Co, ^{152}Eu, ^{228}Th are measured, as well as the background radiation.

During the setup of the electronic devices, the output signal from each device is checked for clarity and consistency with the theoretical background (cf. 2.5) on an oscilloscope which allows us to judge if the devices are adjusted accordingly. An ex-

ample for such an output example is shown in fig. 12. In this case the figure involves the unipolar and the bipolar signal of the main amplifier.

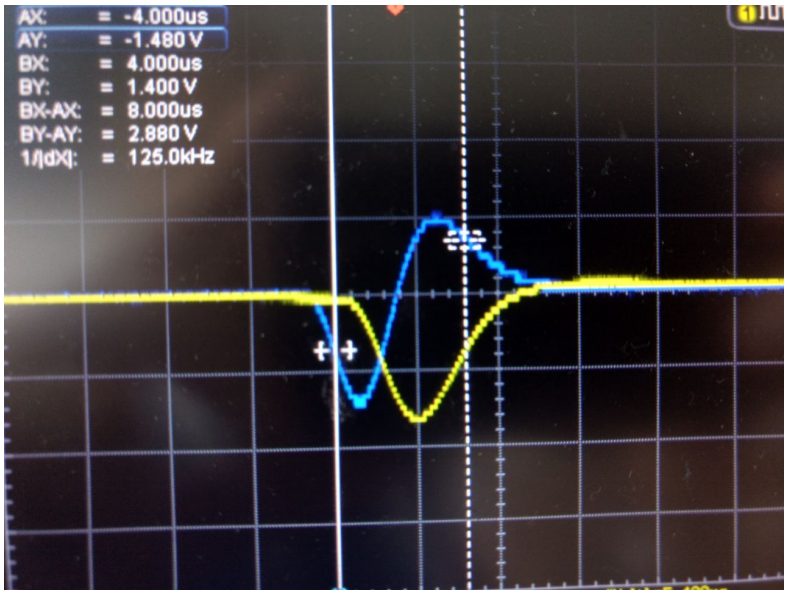

Figure 12: *yellow:* unipolar output signal of the main amplifier. *blue:* bipolar output signal of the main amplifier.

3.2 Angular Correlation

To measure the angular correlation of the pair annihilation photons, the coincidence measurement method is applied. Fig. 13 shows a block diagram representing the electronic circuit of the coincidence measurement. Like in the first part of the experiment, the output signal of each of the electronic devices is checked on the oscilloscope during the setup of the circuit.

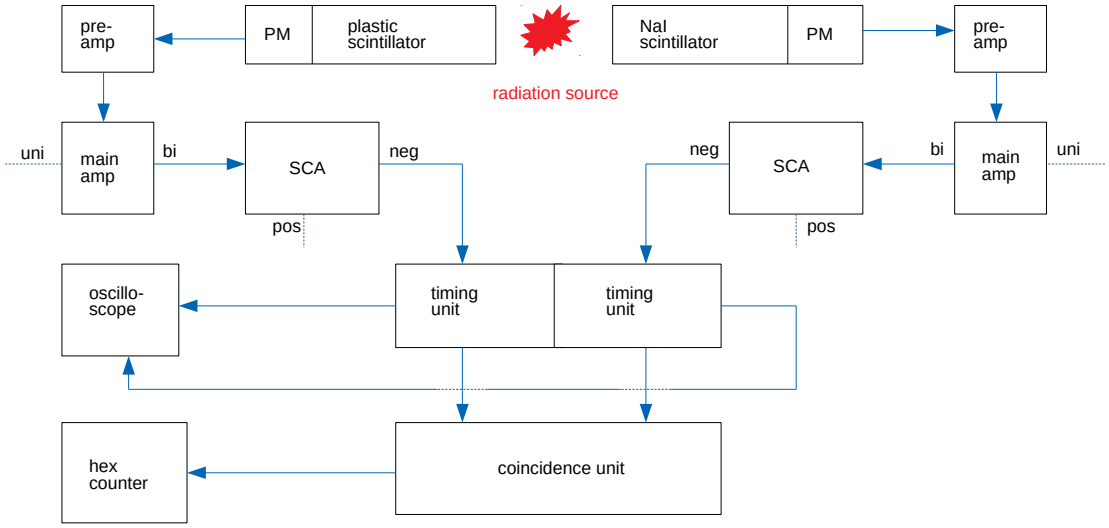

Figure 13: Block diagram representing the electronic circuit for the coincidence measurement

For the coincidence measurement, two different scintillators are used, of which one is an organic plastic scintillator and the other one an inorganic NaI scintillator. The bipolar signal of the main amplifier is sent to the single channel analyzer (SCA). The SCA sends a logical signal to the timing unit if the amplitude of the signal is within an adjustable window. Before the measurement, the upper and lower level each of the two single channel analyzers has to be adjusted so the timing unit only recieves the the signal of the 0.511MeV pair annihilation photons. Therefore the unipolar output signal of the main amplifier is connected to the multi channel analyzer via a gate which is triggered by the positive output signal of the single channel analyzer. Now the γ spectrum, sorted by the multi channel analyzer, is visible on the computer screen like in the first part of the experiment. The upper and lower level are adjusted so that only the signals belonging to the pair annihilation peak reach the multi channel analyzer. This procedure is done with each of the signals from the two respective scintillators.

The ^{22}Na sample is placed in the middle between the two scintillators. The angle between the two scintillators can be adjusted by moving the plastic one on a degree scale around the sample.

When the coincidence unit registers a temporal coincidence between two signals,

it sends a logical signal to the hex counter from which we can read the number of counts within a fixed time interval that is adjusted to 100s at the counter. Starting from 0° on the degree scale (which corresponds to an angle of 180° between the scintillators), the coincidences are counted at various positive and negative angles.

To be able to detect a temporal coincidence of two photons properly, it is made sure that the time the two signals travel from the respective scintillator to the coincidence unit is the same. Therefore the cables connecting the scintillators to their respective timing unit are chosen to have the same length. Also, the delay at the respective SCA is set accordingly to make up for the slower response of the anorganic scintillator.

4 Data Analysis

The data analysis was done with Python 3.5.

4.1 Energy calibration

To determine the spectrum of Thorium, we use the known spectrum of Cobalt, Potassium and Europium for the Channel calibration. Additionally, we subtract the background and derive the count rate n of the data.

$$n = \frac{\text{Counts}_{\text{sample}}}{\Delta t_{\text{sample}}} - \frac{\text{Counts}_{\text{background}}}{\Delta t_{\text{background}}} \tag{15}$$

The times for the measurements were read from the computer and are considered as exact. They can be seen in Table 1.

Sample	Time t [s]
Potassium	2496.977
Cobalt	2550.324
Europium	2402.441
Thorium	56968.111
Background	10800.427

Table 1: Duration of the measurements for the different samples

The error for the Counts N are due to the Poisson distribution of the Counts calculated as $\sqrt{N}$. Therefore the error of the count rate is Calculated as:

$$s_n = \sqrt{\left(\frac{\partial d}{\partial n}\right)^2 \cdot s_N^2 + \left(\frac{\partial d}{\partial N}\right)^2 \cdot s_t^2} = \sqrt{\frac{N}{t^2}} = \sqrt{\frac{n}{t}} \tag{16}$$

The spectra of the samples, as well as the single Fits for their peaks, used for the energy calibration can be found in subsection 6.2. In Python we fitted a Gaussian curve on to the Peaks. The Gaussian Function used for all fits is:

$$G(x) = \frac{A}{\sqrt{2\pi}\sigma} \cdot \exp\left(\frac{(x - Ch)^2}{2\sigma^2}\right), \tag{17}$$

here is x given in 'Channels', and Ch is the position of the maximum. The Channels of the maxima given by the Gaussian fits are used and plotted against the energies of the corresponding peak for calibration. An overview can be seen in Table 2

Sample	Energy [keV]	Channel
Co1	1173.0	941 ± 29
Co2	1332.0	$(1.08 \pm 0.04) \cdot 10^3$
Na1	511	363 ± 34
Na2	1275.0	$(1.02 \pm 0.04) \cdot 10^3$
Eu1	122	142 ± 22
Eu2	344	226 ± 22
Eu3	779	600 ± 29
Eu4	964	760 ± 26
Eu5	1112	879 ± 27
Eu6	1408	1142 ± 35

Table 2: Known Peaks and their respective channel

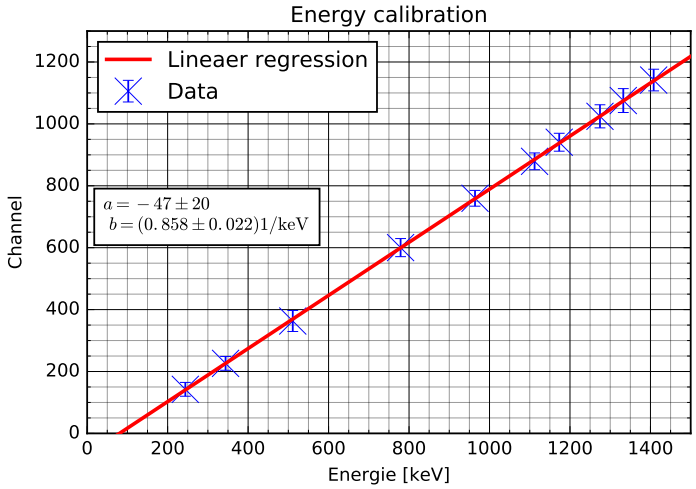

Figure 14: The channel-energie correlation gives together with a linear regression an overall valid formula to convert from channel to energy

With the Linear fit from Figure 14 we obtained the following values:

$$\text{y} - \text{axis interception}: \ a = -47 \pm 20$$
$$\text{slope}: \ b = (0.86 \pm 0.02)\frac{1}{\text{keV}}$$

With the formula

$$E = \frac{\text{Channel} - a}{b} \tag{18}$$

$$s_E = E \cdot \sqrt{\left(\frac{s_a}{c-a}\right)^2 + \left(\frac{s_b}{b}\right)^2} \tag{19}$$

we can calculate the energy for the respective channels.

4.2 Spectrum of Thorium

The complete spectrum of Thorium can be seen in Figure 15, all the peaks are like before fitted with the Gaussian function from Equation 17. The peaks and their fits can be seen in Figure 16,17,18,19,20.

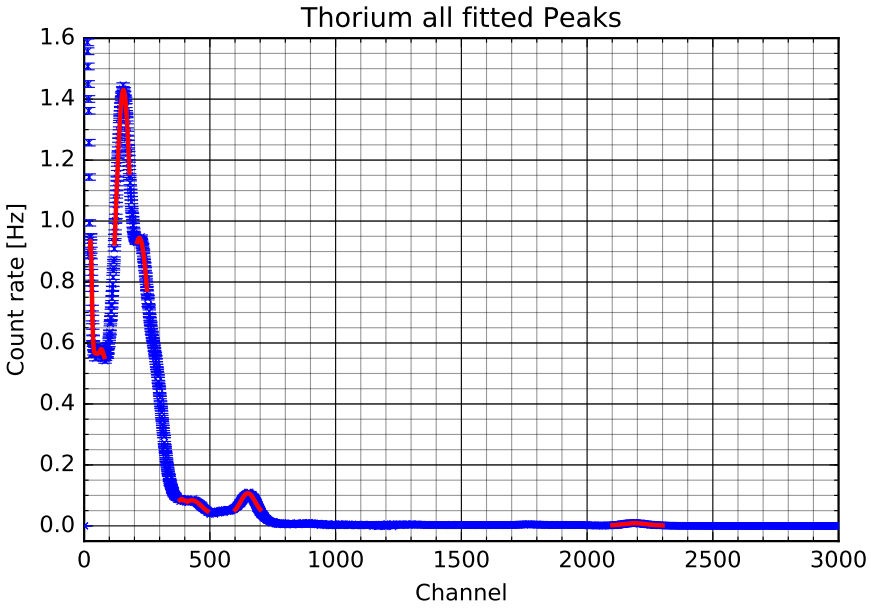

Figure 15: Complete spectrum of the Thorium decay

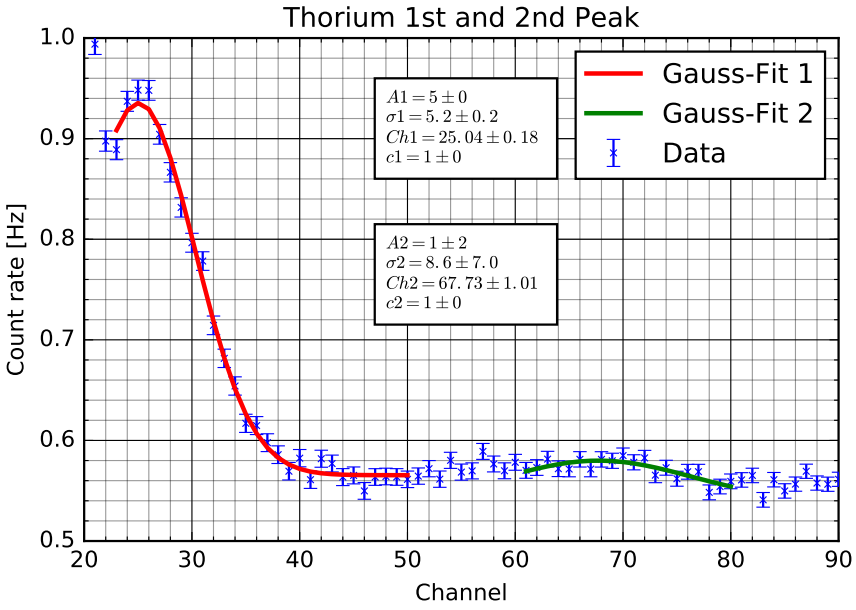

Figure 16: Thorium peaks 1 and 2

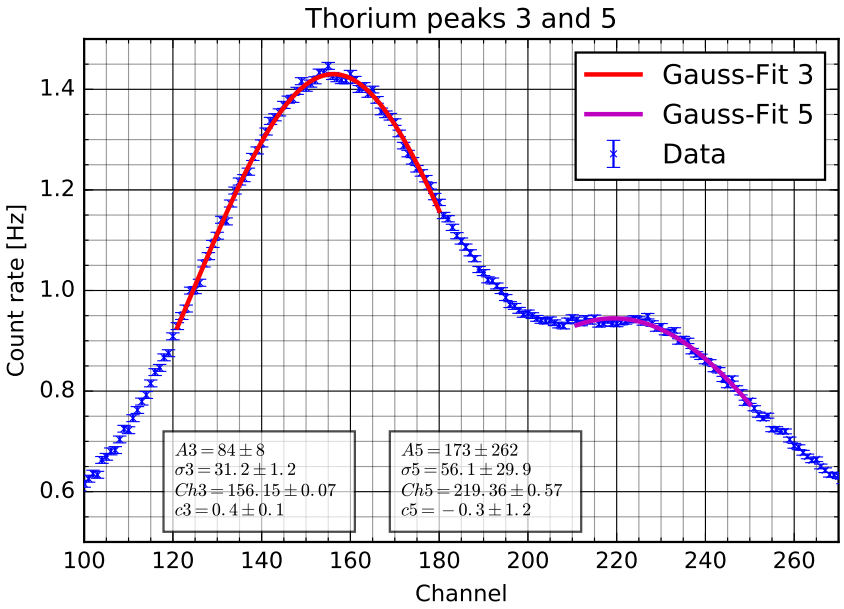

Figure 17: Thorium peaks 3 and 5

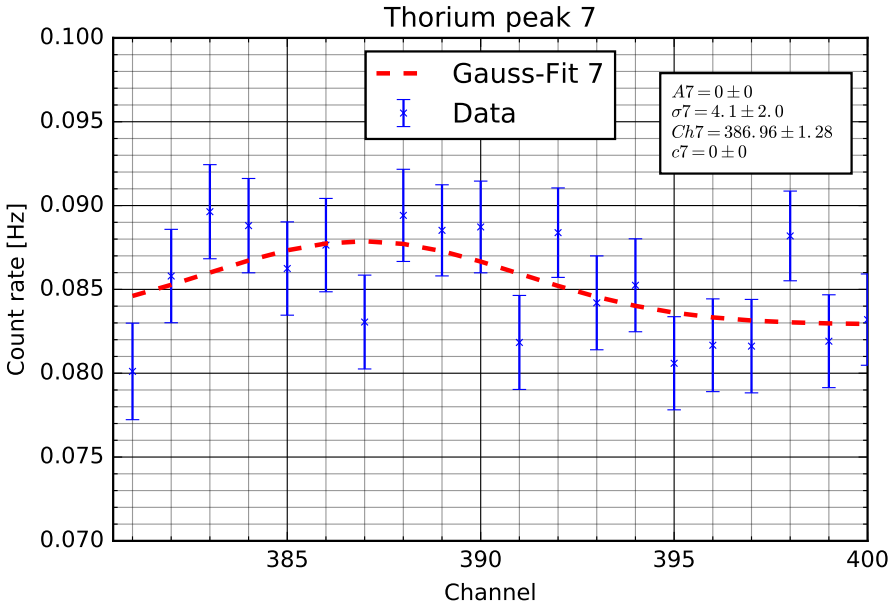

Figure 18: Thorium peak 7

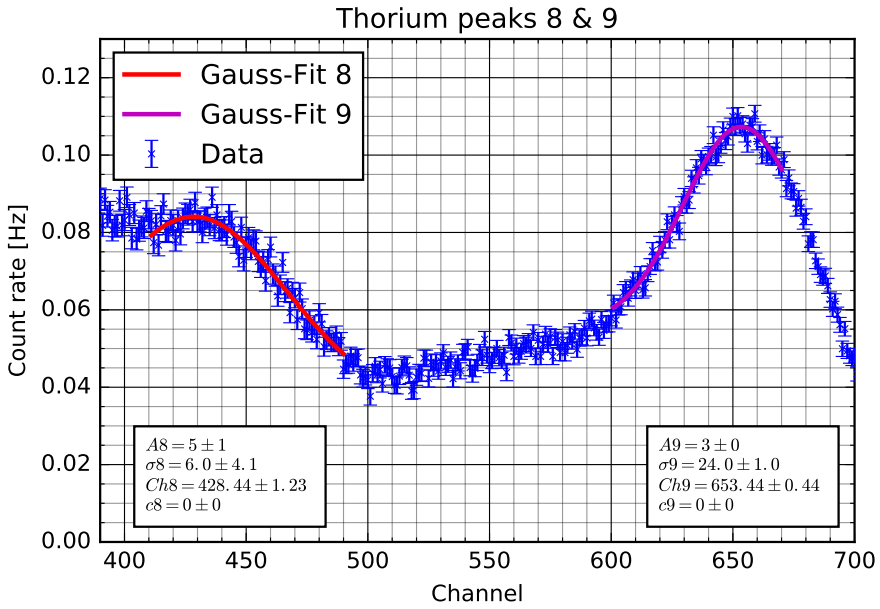

Figure 19: Thorium peaks 8 and 9

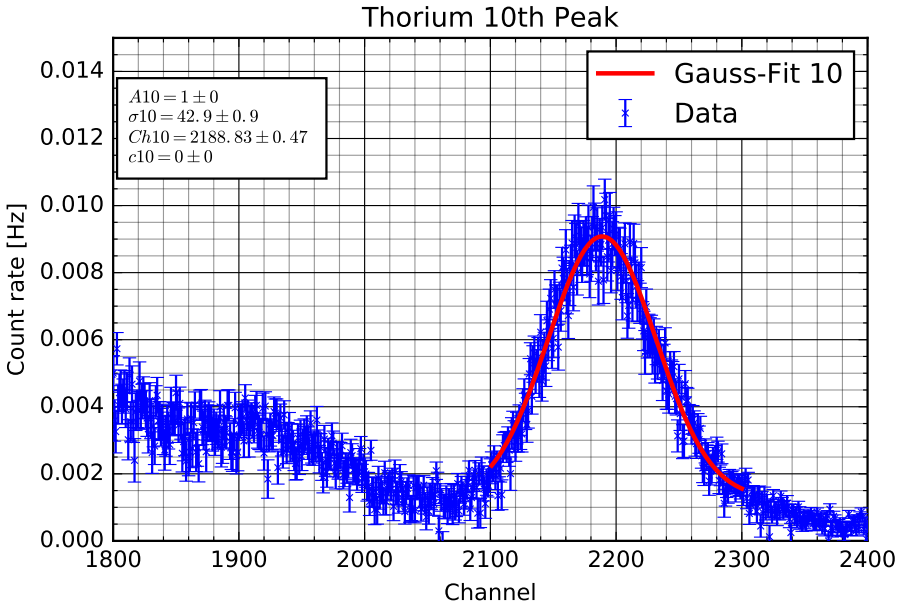

Figure 20: Thorium peak 10

From the positioning of the peaks and with Equation 18 we obtain the energies which can be seen in Table 3. It was not possible for us to find for each reference decay the peak of the spectrum.

Peak	Channel	Energy[keV]	Decay	E_{ref}[keV]
1	25.0 ± 0.2	84 ± 6	^{228}Th$\rightarrow^{224}$Ra	84.4
2	68 ± 1	134 ± 11	^{228}Th$\rightarrow$ ^{224}Ra	131.61
3	156.15 ± 0.07	236 ± 36	^{212}Pb$\rightarrow$ ^{212}Bi	238.99
4			^{224}Ra$\rightarrow$ ^{220}Rn	240.99
5	219.4 ± 0.6	310 ± 65	^{212}Pb$\rightarrow$ ^{212}Bi	300.03
6			^{212}Bi$\rightarrow^{212}$Po	452.98
7	387 ± 1	506 ± 14	^{208}Tl$\rightarrow$ ^{208}Pb	510.77
8	428 ± 1	554 ± 46	^{208}Tl$\rightarrow$ ^{208}Pb	538.19
9	653.4 ± 0.4	816 ± 35	^{216}Po$\rightarrow$ ^{212}Pb	804.90
10	2188.8 ± 0.5	2605 ± 83	^{208}Tl$\rightarrow$ ^{208}Pb	2614.53

Table 3: The Peaks and their Energies in comparison to the guessed decays. The decays can be found in subsection 6.1

4.2.1 Coincidence Measurement

For different angles we measured 511 keV-photons with both scintillators. The error on the angle is guessed to $s_{angle} = 0.1$ and like in subsection 4.1 explained, the mistake on the counts N is given trough $s_N = \sqrt{N}$. We measured 100s for each angle, the number of coincidences can be seen in Table 4. Because we expect a gaussian distribution around the 0° angle we fitted the data in Figure 21.

Angle [°]	Counts
-95.0 ± 0.1	62.0 ± 8.0
-90.0 ± 0.1	65.0 ± 8.0
-75.0 ± 0.1	82.0 ± 9.0
-65.0 ± 0.1	84.0 ± 9.0
-55.0 ± 0.1	72.0 ± 8.0
-45.0 ± 0.1	100.0 ± 10.0
-35.0 ± 0.1	93.0 ± 10.0
-25.0 ± 0.1	87.0 ± 9.0
-20.0 ± 0.1	103.0 ± 10.0
-15.0 ± 0.1	121.0 ± 11.0
-10.0 ± 0.1	143.0 ± 12.0
-5.0 ± 0.1	1081.0 ± 33.0
-3.0 ± 0.1	1367.0 ± 37.0
-2.0 ± 0.1	1481.0 ± 38.0
-1.0 ± 0.1	1540.0 ± 39.0

Angle [°]	Counts
0.0 ± 0.1	1614.0 ± 40.0
1.0 ± 0.1	1520.0 ± 39.0
2.0 ± 0.1	1564.0 ± 40.0
3.0 ± 0.1	1437.0 ± 38.0
5.0 ± 0.1	1218.0 ± 35.0
10.0 ± 0.1	189.0 ± 14.0
15.0 ± 0.1	126.0 ± 11.0
20.0 ± 0.1	103.0 ± 10.0
25.0 ± 0.1	98.0 ± 10.0
35.0 ± 0.1	107.0 ± 10.0
45.0 ± 0.1	83.0 ± 9.0
55.0 ± 0.1	73.0 ± 9.0
65.0 ± 0.1	78.0 ± 9.0
75.0 ± 0.1	73.0 ± 9.0
90.0 ± 0.1	50.0 ± 7.0
95.0 ± 0.1	90.0 ± 9.0

Table 4: The counts of coincidences in comparison to the angle between the scintillators

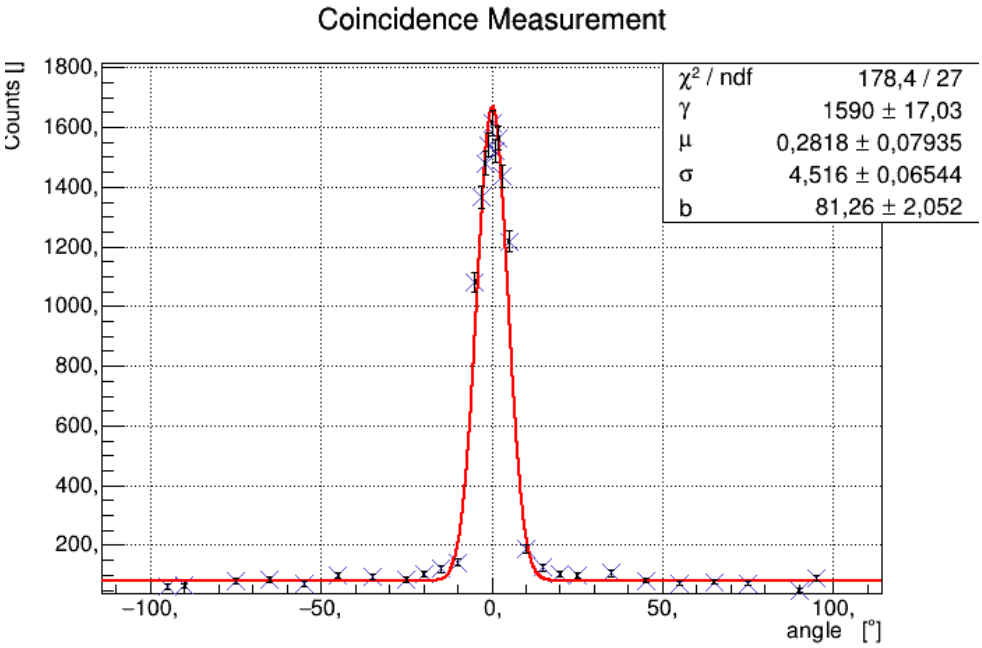

Figure 21: The fitted data of the coincidence measurement

5 Summary and Discussion

It was possible to calibrate the MCA-unit with the known spectra of Potassium, Cobalt and Europium to detect 8 of the 10 major peaks in the spectrum of the Thorium decay. It was possible to match those peaks to decays within the Thorium decay chain. We were not able to find the peaks of the ^{224}Ra decay (240.99 keV) as well as the ^{212}Bi decay (452.98 keV). All matched values lie within 1 σ of the given literature value. We noticed a Peak at Channel 1992 which corresponds to an energy of $\sim$ 1396 keV in the background measurement which we could relate to a ^{40}K decay from either the 'Long half life experiment' which is run across the aisle or the natural occurrence of ^{40}K in the air and humans or both. In Figure 28 one can get a good glimpse at the peaks produced by the Compton scattering between Channels 250 and 800.

With the coincidence Measurement we could confirm, that two photons are produced in electron-positron pair annihilation and drift apart at an angle of 180°. The offset of $(0.28 \pm 0.07)°$ to 0 is within 4 and given by the Gaussian fit. It can be explained by the fact, that both scintillators were mounted on two different tables which probably were not quite parallel to one another.Furthermore one could minimize this error by mounting everything on to one table.

6 Appendix

6.1 γ peaks of the ^{228}Th decay chain

Nucleus	E_γ [keV]	Relative Intensity [ ]
^{228}Th	84.4	1000
^{228}Th	131.61	107
^{228}Th	166.41	84.9
^{228}Th	215.89	207.8
^{224}Ra	240.99	4.1
^{212}Pb	238.63	100
^{212}Pb	300.09	7.57
^{212}Bi	452.98	1.01
^{208}Tl	510.77	22.8
^{208}Tl	538.19	85.2
^{216}Po	804.9	0.002
^{208}Tl	2614.53	100

Table 5: Relevant γ peaks of the ^{228}Th decay chain [2]

6.2 Fits of the Peaks

6.2.1 Background

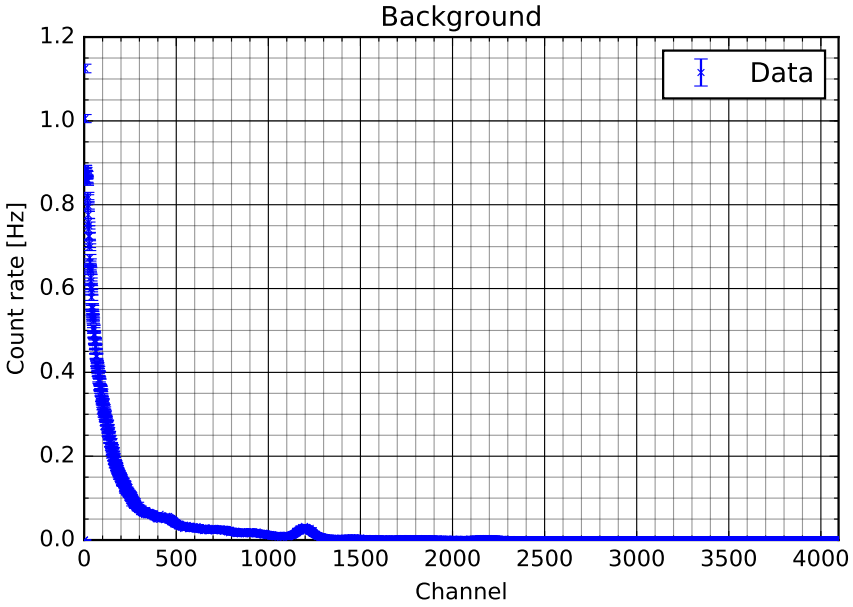

Figure 22: Background measurement

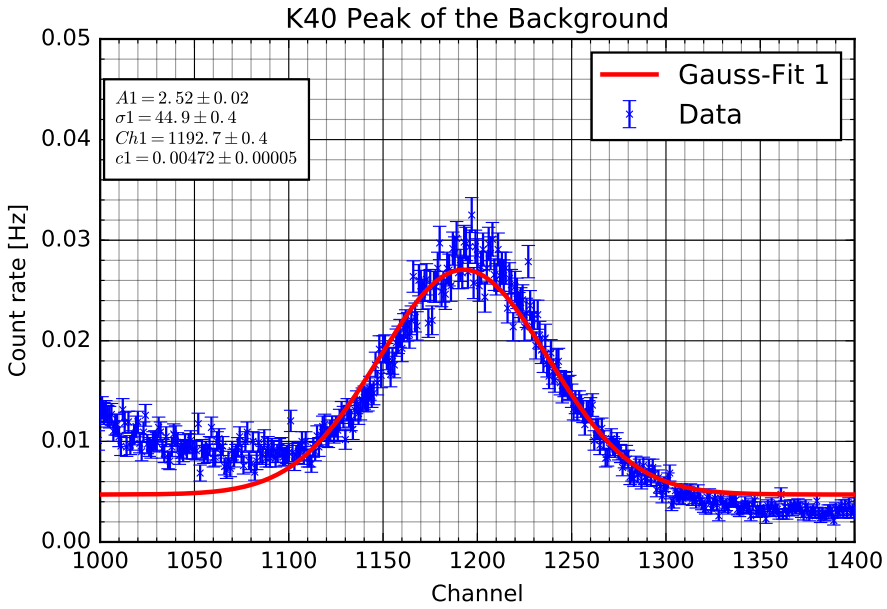

Figure 23: ^{40}K Peak in the Background spectrum

6.2.2 Potassium

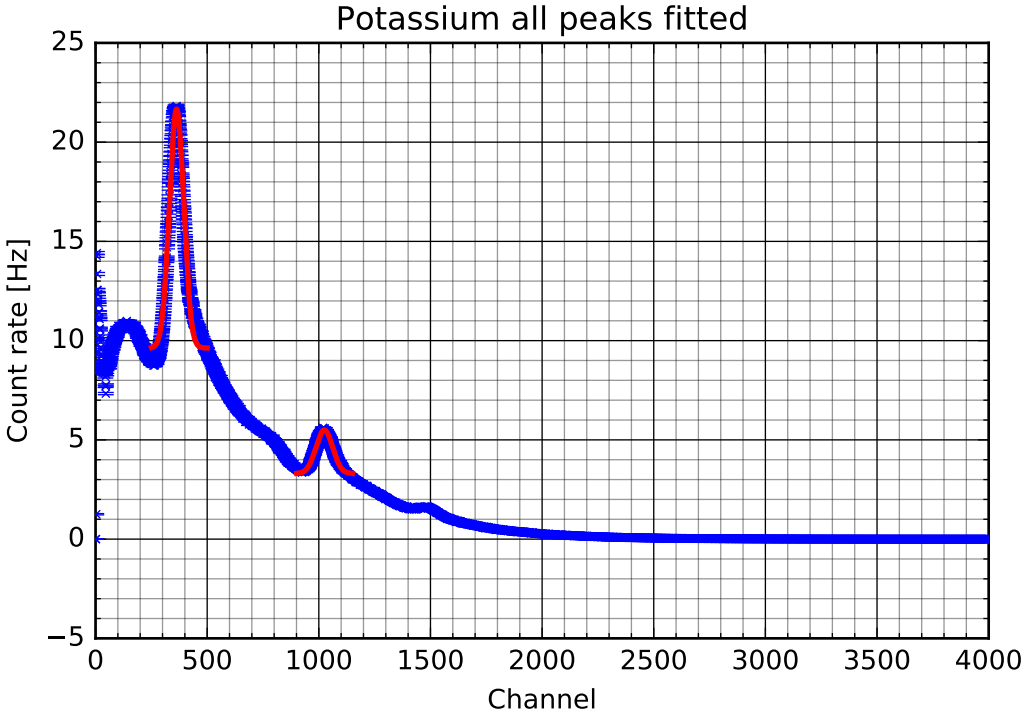

Figure 24: The complete Potassium spectrum with the fitted peaks

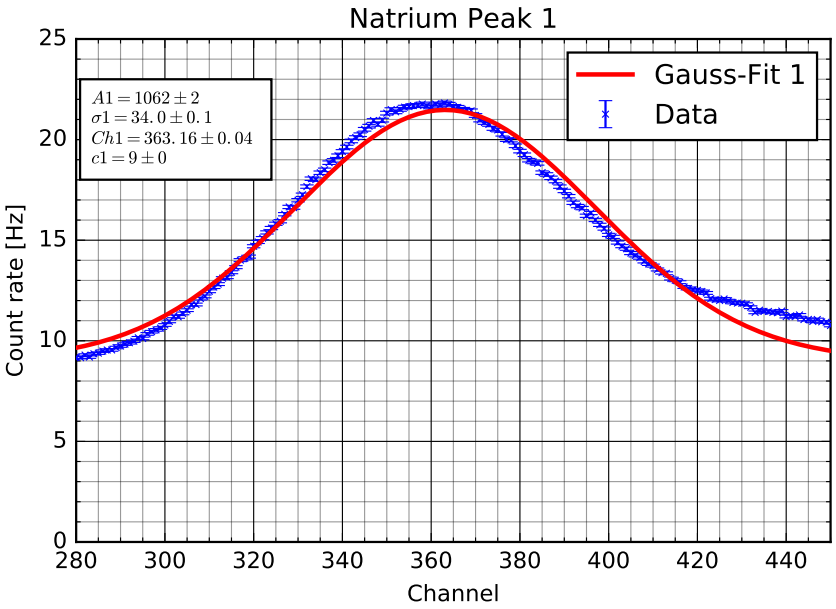

Figure 25: The first Potassium peak with Gaussian fit

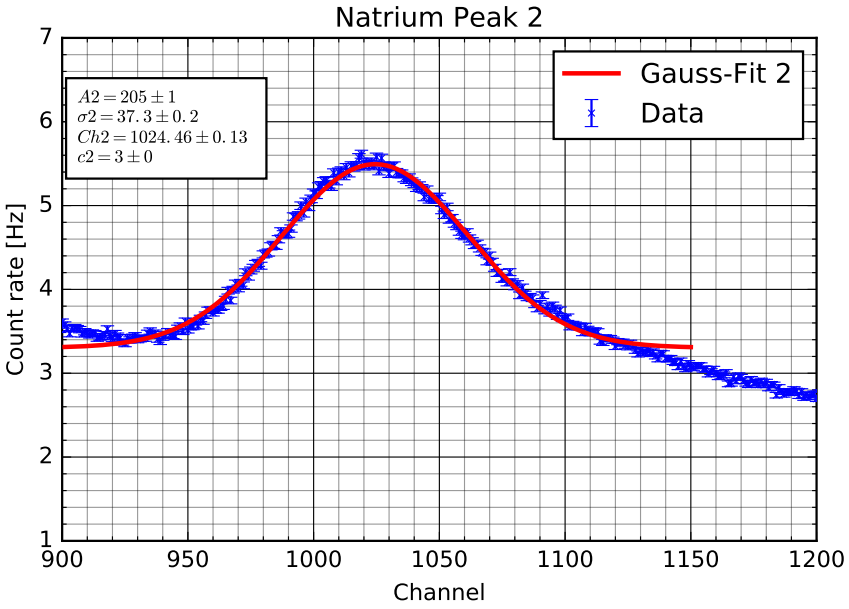

Figure 26: The second Potassium peak with Gaussian fit

6.2.3 Cobalt

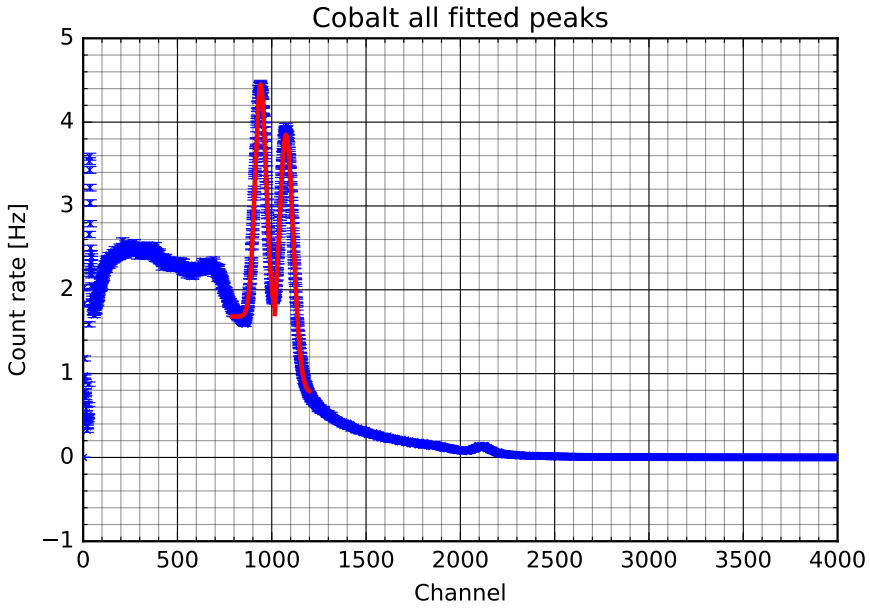

Figure 27: The complete Cobalt spectrum with the fitted peaks

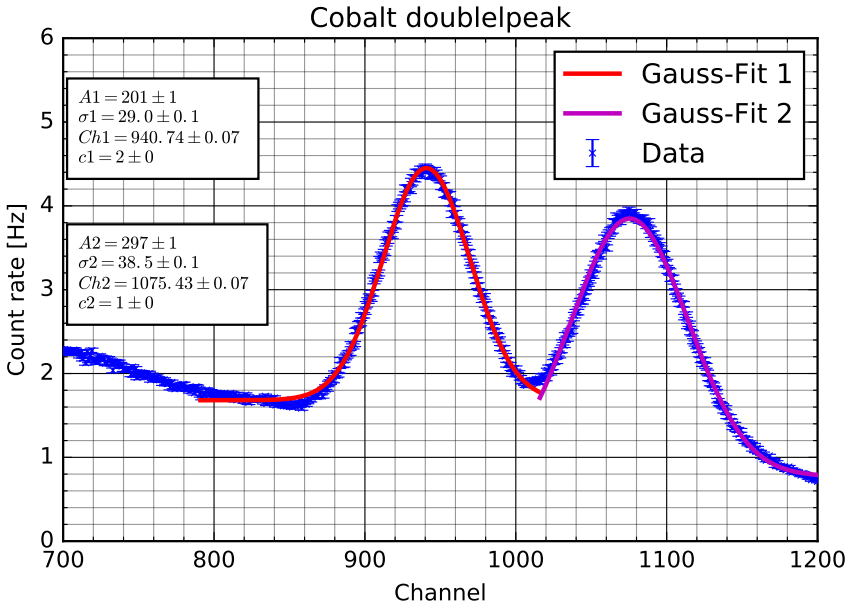

Figure 28: The Cobalt doublepeak with the two fitted Gaussians

6.2.4 Europium

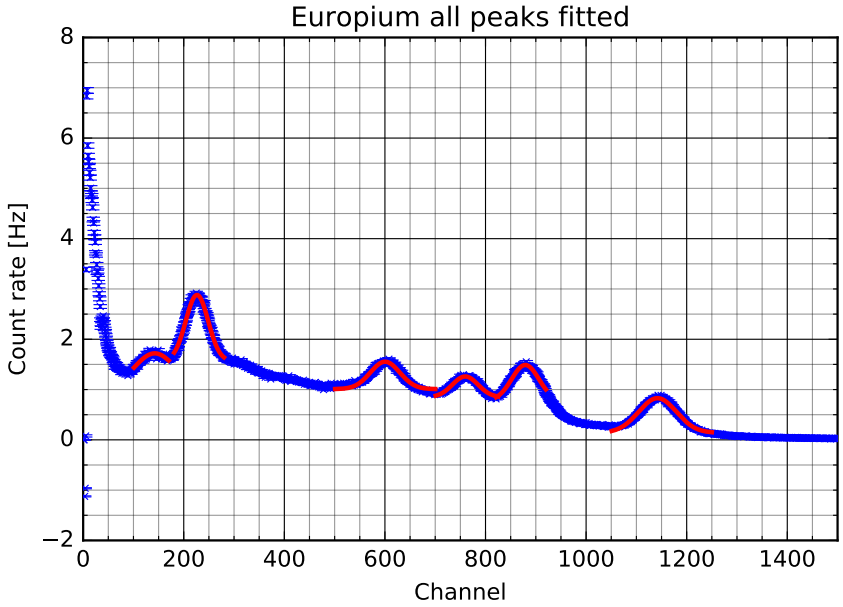

Figure 29: The complete Europium spectrum with the fitted peaks

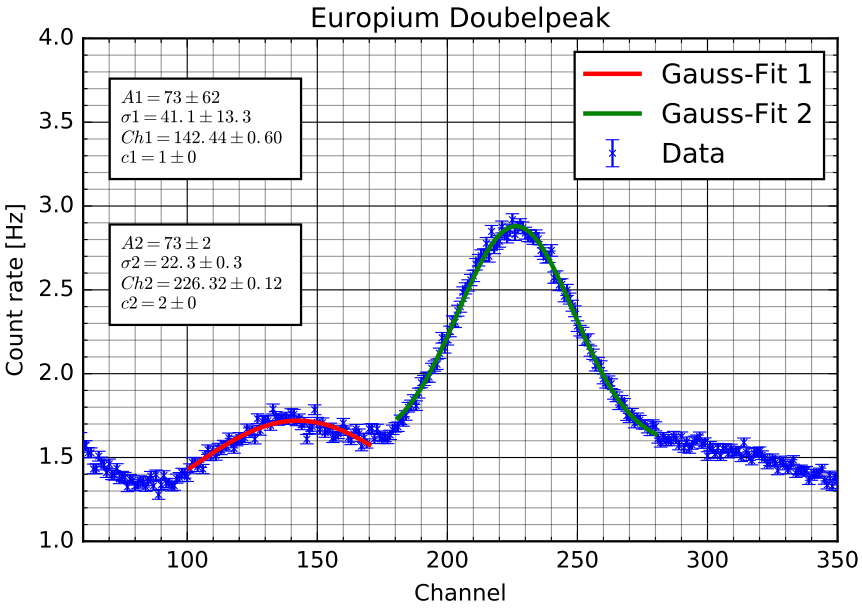

Figure 30: The first two peaks of the Europium spectrum with fitted Gaussians

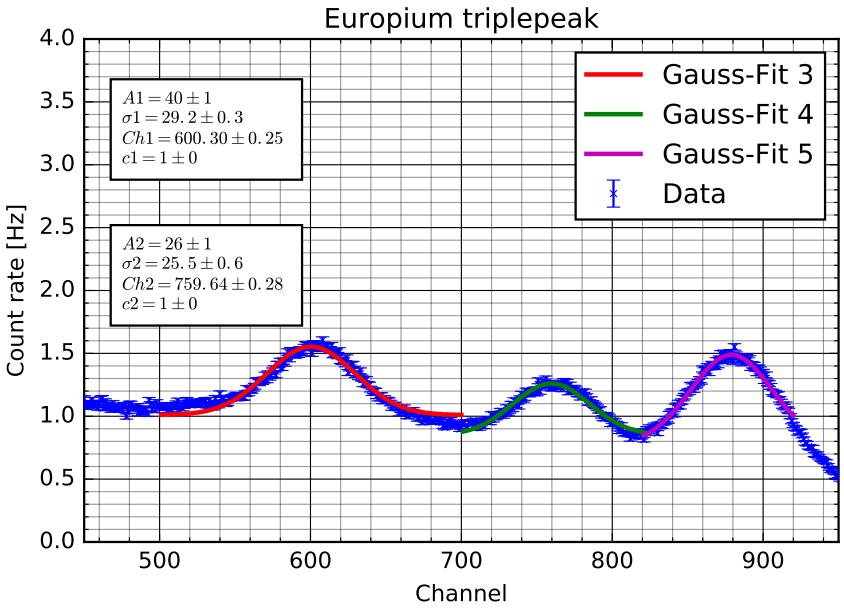

Figure 31: Peaks 3,4 and 5 of the Europium spectrum with fitted Gaussians

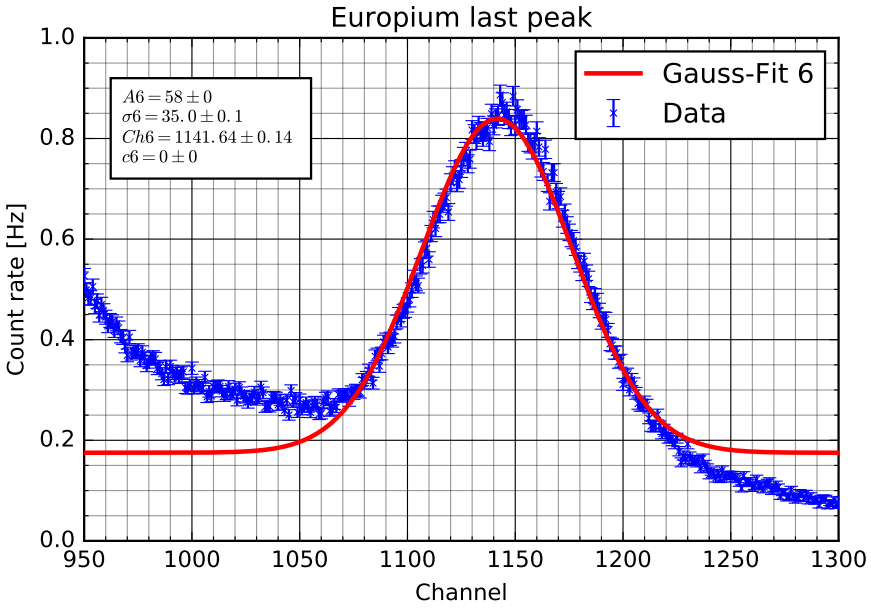

Figure 32: The 6th peak of the Europium spectrum with fitted Gaussian

6.3 Lab Notes

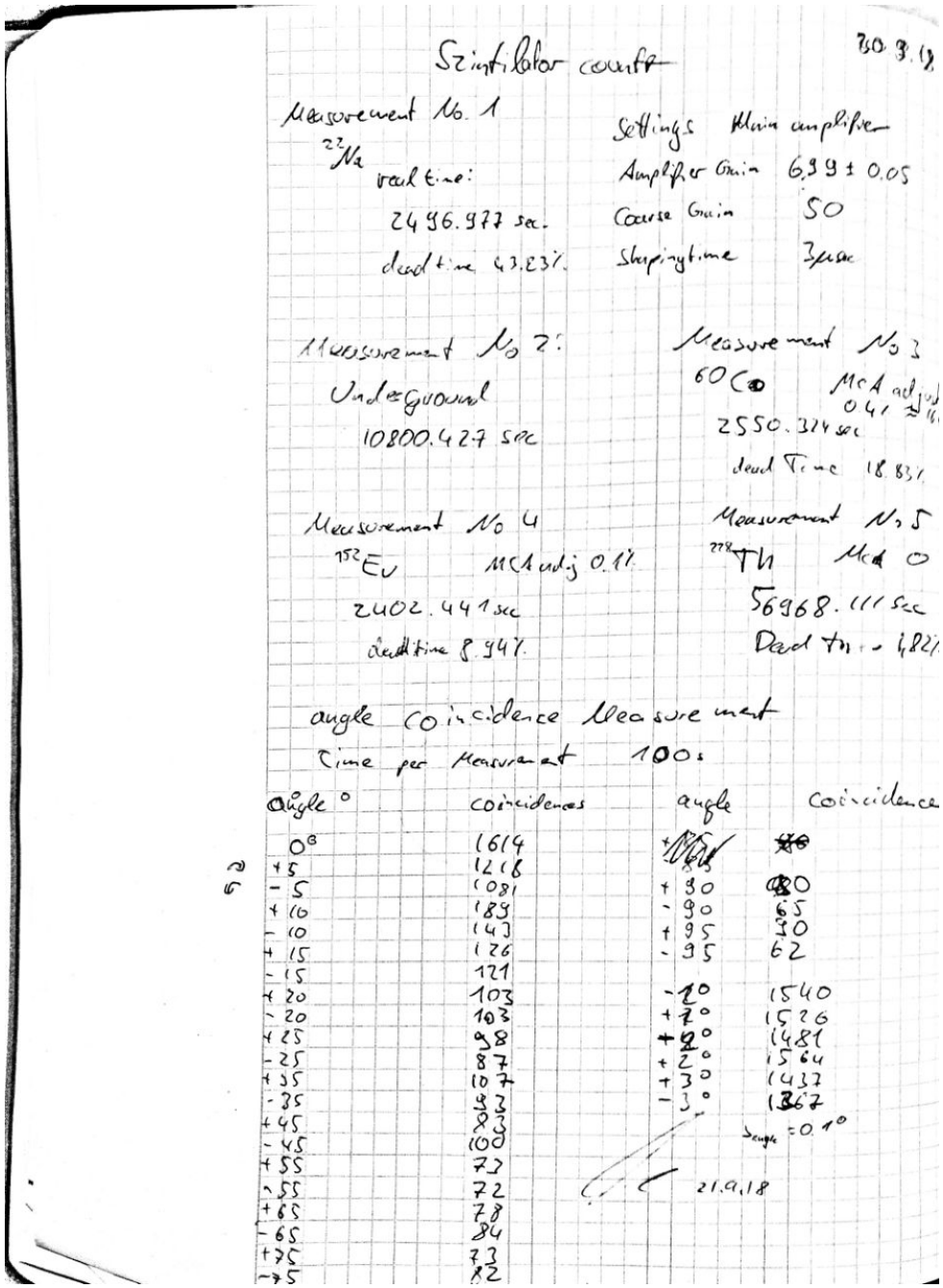

Szintillator counts 30.3.18

Measurement No. 1
^{22}Na
real time:
2496.977 sec.
dead time 43.23%

Settings Main amplifier
Amplifier Gain 6.99 ± 0.05
Course Gain 50
Shaping time 3 µsec

Measurement No 2:
Underground
10800.427 sec

Measurement No 3
^{60}Co MCA adj 0.41
2550.314 sec
dead Time 18.83%

Measurement No 4
^{152}Eu MCA adj 0.1%
2402.441 sec
deadtime 8.94%

Measurement No 5
^{228}Th MCA 0
56968.111 sec
Dead Time 4.82%

angle coincidence Measurement
Time per Measurement 100s

Angle °	coincidences	angle	coincidence
0°	1614		
+5	1216		
-5	1081	+30	80
+10	189	-90	65
-10	143	+95	90
+15	126	-95	62
-15	121		
+20	103	-10	1540
-20	103	+10	1526
+25	98	+20	1481
-25	87	+20	1564
+35	107	+30	1437
-35	93	-30	1367
+45	83		
-45	100		
+55	77		
-55	72		
+65	78		
-65	84		
+75	73		
-75	82		

Δangle = 0.1°

21.9.18

References

[1] Th. Klapdor-Kleingrothaus, *Versuchsanleitung Fortgeschrittenen Praktikum Teil I: Szintillationszähler. Universität Freiburg im Breisgau*, 9.Jan 2017

[2] Tobijas Kotyk, *Versuche zur Radioaktivität im Physikalischen Fortgeschrittenen Praktikum an der Albert-Ludwigs-Universität Freiburg*, Zulassungsarbeit, Universität Freiburg im Breisgau, 16.11.2005

[3] Physikalisches Fortgeschrittenen-Praktikum I: Szintillationszähler, Appendix: Theorie und Geräte. Universität Freiburg im Breisgau, 01.09.2005

[4] `https://c1.staticflickr.com/5/4061/4706688476_8a083bcdcf.jpg`

[5] `http://www.people.vcu.edu/~mhcrosthwait/clrs322/images/gammaspectrum.jpg`

[6] `http://www.tpub.com/doeinstrument/instrumentation%20and%20control_files/image237.jpg`

[7] `https://www.lasercomponents.com/fileadmin/user_upload/home/Images/LCP/Photomultiplier-Grafik.jpg`